ACQUIRING UNIAXIAL STRESS-STRAIN CURVE BY FAST FINITE ELEMENT ANALYSIS FOR CHARACTERIZATION OF WHOLE-CELL ELASTIC PROPERTY

by

Haitao Yang

Bachelor of Science, Harbin Institute of Technology, China, 2011

Submitted to the Graduate Faculty of

Swanson School of Engineering in partial fulfillment

of the requirements for the degree of

Master of Science in Electrical Engineering

University of Pittsburgh

2013

UNIVERSITY OF PITTSBURGH

SWANSON SCHOOL OF ENGINEERING

This thesis was presented

by

Haitao Yang

It was defended on

November 21, 2013

and approved by

Guangyong Li, Ph.D., Associate Professor

Department of Electrical and Computer Engineering

Ervin Sejdic, Ph.D., Assistant Professor

Department of Electrical and Computer Engineering

Mingui Sun, Ph.D., Professor

Department of Electrical and Computer Engineering

Thesis Advisor: Guangyong Li, Ph.D., Associate Professor

ACQUIRING UNIAXIAL STRESS-STRAIN CURVE BY FAST FINITE ELEMENT ANALYSIS FOR CHARACTERIZATION OF WHOLE-CELL ELASTIC PROPERTY

Haitao Yang, M.S.

University of Pittsburgh, 2013

An understanding of whole-cell elastic property can provide insight into cellular response to mechanical loading. Hertz model is often used to extract the Young's modulus from the atomic force microscopy (AFM) force indentation depth curve (F-D curve) for characterization of cell's elastic property. However, Hertz model is only relatively accurate when the sample can be regarded as infinite half space and its material is linear elastic, which is contradictory with the fact that cell is usually very thin and cell's elastic properties are considered to be highly nonlinear, especially when the deformation is very large. Finite element analysis can be used to handle the nonlinear elastic property and large deformation by using the hyperelastic model to model the cell material. However, previous studies have not demonstrated a convenient way to search for the model parameters that can fit the experimental data. In this paper, we put forward a method based on finite element analysis. Our new method adopts a general uniaxial stress-strain curve (associated with a hyperelastic model) to represent cell's material and uses a recursive method to search for this uniaxial stress-strain curve by minimizing the difference between the experimental and simulated F-D curve. This new recursive approach not only offers a high match accuracy between the experimental and simulated F-D curve(error rate less than 5% is ready to be obtainable), but also minimizes the number of recursions in searching for the stress-strain curve(less than 10 recursions are enough for the good enough match in normal situation).

TABLE OF CONTENTS

LIST OF FIGURES

1.0 INTRODUCTION

Numerous pathophysiological processes, such as inflammation, certain forms of cancer and cardiovascular disease, have reported to be closely related to the changes of cell or tissues' mechanical properties [1-4]. AFM indentation experiment is used to study breast cancer cells in Ref [5]. Cell mechanical phenotype is tried by Lekka's group [6] to recognize cancer cells. The application of AFM to the cancer cell detection has been discussed by M.Lenka and P.Laidler [7]. The variation of cell's elasticity property is reported to be the comprehensive results of the cytoskeleton structure remodeling because of the exterior stimuli or environment changes; the changes of cell elasticity has been adopted by more and more researchers to identify the cells in different conditions or groups. But extracting relatively accurate cell elasticity information is not an easy job. The application of cell's elastic property has been limited by both the methods to characterize the cell's elastic property and the difficulty to do the well-controlled experiments. The well controlled experiments depend on the available instruments and fine samples you can get; the accuracy you can place the AFM tip onto the cell surface depends on the visualizing system and the controllability of the instrument; the normal biological samples may also be in different states and then show different elastic properties, thus the reliability of the comparison depends on how well you can control your experiments and the samples you prepare. The method to estimate the whole-cell elastic property from experimental F-D curve is equally important, a lot of factors can affect the measured F-D curve, which includes the cell size, nonlinear property of cell material

property and so on, but the popular Hertz model fitting method ignores both the shape information and the nonlinear material property. Estimation of cell's elastic property from the measured F-D curve is an inverse problem, so including as much available information into the model as possible can help improve the estimation accuracy. Here in this thesis, we focus on developing a new algorithm to estimate the cell's elastic property from the F-D curve rather than discussion about how to design the well-controlled experiments. The new method is a revised version of the current finite element analysis method for cell elastic property estimation; by this new method, the computational cost is largely reduced and the fitting accuracy between simulation and experimental F-D curve is also improved to a higher level.

The second chapter of this thesis introduces the basic principles of Atomic Force Microscopy (AFM) and its application for indentation experiments; then the current available algorithms for estimation cell elastic property are reviewed. In the third chapter, the new method is presented and discussed. The experiments process, results and discussion is shown in the fourth chapter, the detailed mechanism of our new algorithm is discussed.

2.0 BACKGROUND

2.1 ATOMIC FORCE MICROSCOPY FOR MICRO-INDENTATION

2.1.1 Basic Atomic Force Microscopy principle

Atomic Force Microscopy (AFM) is a powerful technique to measure extremely small force and construct high-resolution image of various surface in liquid or air environment. Its unique capabilities has made it an indispensable tool to study the mechanical property of biological sample including various soft tissues and cells. The basic working principle of AFM is briefly introduced in the following part.

AFM detects very minute force (in the Pico newton level) by a very soft cantilever (spring constant approximately ranges from 0.01 N/m to 60 N/m) and the amplification of the long laser light path. The schematic of basic AFM working principle is pictured in Figure 1. As the AFM approaches or contacts the sample surface by the tip on the very end of the cantilever, the attractive force or repulsive force will cause the AFM cantilever to bend down or up, then the position of the laser spot on the photo detector will change, which will be transformed into electrical signal transmitting into the control system. The distance between laser generator and the cantilever and the distance between the cantilever and photo detector are long enough to amplify the very small deflection of the cantilever. Then the deflection of the cantilever is transmitted into the control

system to do the feedback and all the signals are also transmitted into the computer to show the measurement results out.

AFM works in a lot of modes, such as contact mode, tapping mode, force modulation mode. Force modulation mode is utilized to indent the sample surface to get the F-D curve. Figure 2 shows a typical force-displacement curve, the force is zero when the tip is far away from the sample surface; it is attractive force when the tip is very close to the sample but not in contact, ; after the tip contacts the sample surface, it becomes repulsive force and increases very quickly as the tip contacts the sample [8].

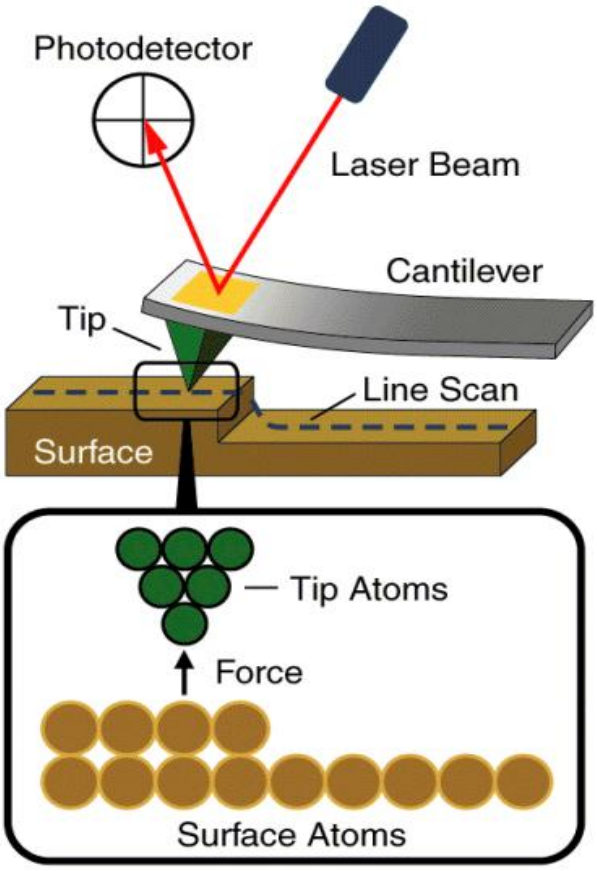

Figure 1.Schematic of a typical AFM [9]

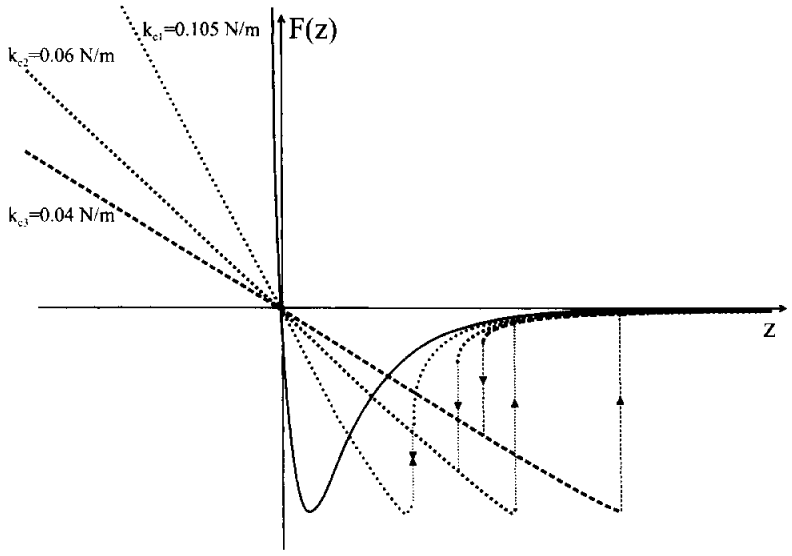

Figure 2. Force-displacement curves for cantilever with different spring constant [8]

2.1.2 **Blunt sphere tip for whole-cell elastic property and sharp tip for local elastic property**

When using AFM to indent the sample, two different kinds of probes can be used, sharp tip in Figure 3 and large blunt sphere tip in Figure 4. The sharp tip's shape can be cone, pyramid or hemisphere; the radius is usually in the range from 10 nm to several dozens of nanometers; this kind of tip can be used for the high-resolution imaging of sample surface and can also be used to measure the local elastic property of the cell surface because of its high-lateral resolution and also can construct an elastic property mapping of the sample surface's elastic property [12]. Ref [13, 14] has used microsphere tip to distribute the stress onto the sample surface, the microsphere's radius is usually in the micrometers level, so its lateral resolution is too low to measure the sample topography; in the other hand the microsphere's size is in the same level with cell's size, so large indentation depth can be done by this microsphere without penetrating the cell surface.

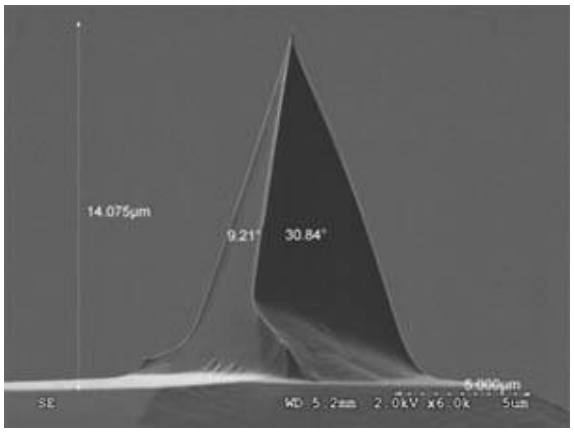

Figure 3. SEM Micrograph of a pyramid-shape tip [10]

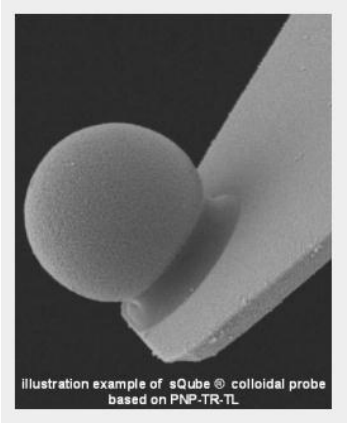

Figure 4. Au sphere tip [11]

The local elastic property is usually measured by using a sharp tip with radius about dozens of nanometers, and the indentation depth is usually very small. Small indentation depth makes it satisfy Hertz model's infinite half space assumption; and this small indentation also did not cause large change of the cytoskeleton, so the material can be assumed to be linear elastic; thus, it satisfies the assumptions of Hertz model. According to my simulation, if a cone tip with radius 50 nm indents the sample which is 7 um thick and linear elastic with Young's modulus 1 kPa, the estimated modulus according to Hertz model is 981 Pa which is quite accurate. But in practical

experiments, the estimation results may be not accurate at all. One of the reasons may be that the sharp probe has penetrated into the cell, but not pressing an elastic material; so the contact area in realistic experiment is much different from the ideal modeling of the Hertz model. In Ref [15], it has been shown that for a very soft probe (sprint constant k=0.065) to scan the cell surface in tapping mode; when the indentation depth increases 20 nm, the cantilever oscillation amplitude decreases only about 1 nm. This experiment observation shows that because the cell surface is very soft and the tip is very sharp and rigid, the tip may penetrate into the cell. When the indentation depth is large, the penetration depth will be larger, which results in the large inaccuracy of Hertz model.

The whole cell elastic property cannot be represented by the local elastic property; firstly it varies a lot in different regions of the cell, as shown in Ref[16], before the "Bottom Effect" correction, the maximum Young's modulus can be 100 times of the minimum Young's modulus measured in different regions of the same cell, even after the "Bottom Effect" correction, the difference in the two very close regions in the approximately center of the cell can be about 10 times. By Comparison of the cancerous cell's region with largest young's modulus with the normal cell's region with smallest Young's modulus, the wrong conclusion that the cancerous cell's elastic modulus is larger than the normal cell's elastic modulus may be derived. So comparison of local elastic property of two different cells may be not very reliable. For whole-cell elastic property measurement, sphere tip with radius of several micrometers will be used to indent the center the cell, and the whole cell's cytoskeleton will contribute into the measurement. So the whole-cell elastic property will be more consistent to represent the cell's elastic property than the local elastic property. Thus the measurement of whole-cell elastic property is the focus of this thesis.

However, the measurement and characterization of whole-cell mechanical behavior has received very limited attention. In Ref [17], three characterization methods including Hertz contact theory, an exponential equation and a parallel-spring recruitment model are shown to measure and characterize the whole cell elastic property. Figure 5 shows a typical experimental force-indentation curve and their description by the above mentioned three characterization methods.

Figure 5 shows Hertz contact theory's limited ability to describe the experimental force-indentation curve, while the exponential equation and PSR model can fit the experimental force-indentation curve quite well. But this good fitting does not mean that the two models can describe the cell materials because the experimental curve is the product of the both cell geometry and cell materials. But these two models all ignores the cell geometry factors and only consider the cell materials. Obviously, this is not correct and the following part 2.4 will show cell geometry's influence on the final F-D curve.

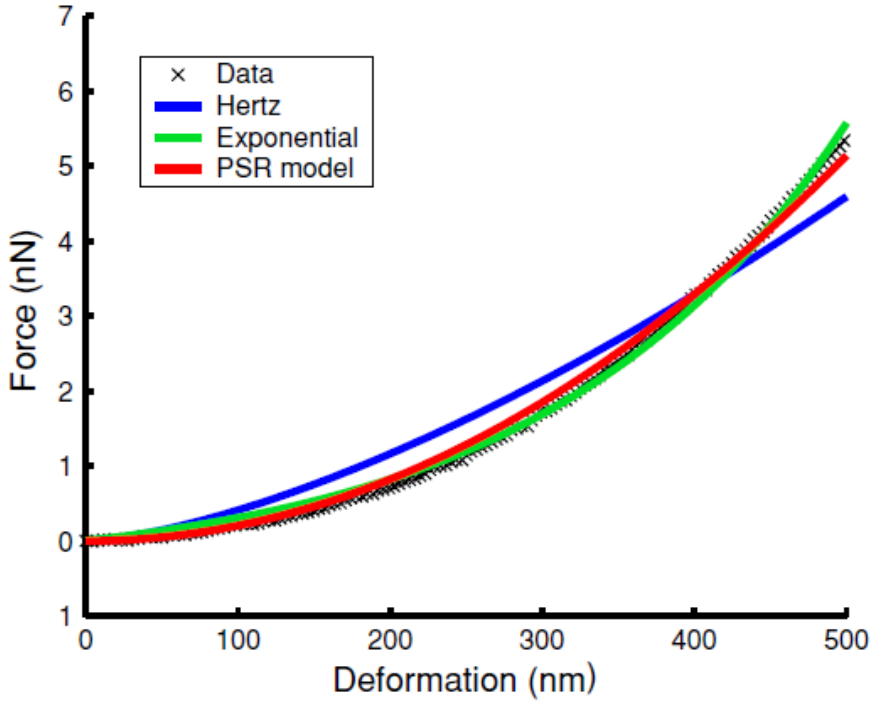

Figure 5. Typical force-indentation curves and their description by three characterization methods [17]

2.2 HERTZ MODEL FOR CHARACTERIZING CELL ELASTIC PROPERTY

Up to now Hertz model has still been the most popular model to estimate the cell elastic property. But the original Hertz model is designed to be used to model the simple case of two perfect homogeneous smooth body pressing each other [18]. It at least replies on two important assumptions in application for AFM probing cell, (1) the cell is assumed to be isotropic, infinite half space; (2) Cell material is homogeneous and linear elastic. Since cell is very small, in order to fulfill the first assumption, the deformation should be small enough (at least less than 10% of the cell thickness) so that this deformation can be neglected compared with the cell thickness. However, indentation larger than 400 nm should be used in order to avoid the uncertainty of the probe-sample contact point [19], which seems to be a controversy with the small indentation requirements. But Hertz model is still used in many situations despite of this invalid assumption which could result in that the estimated cell modulus relies on the thickness of the cell and compliance of the substrate, the more rigid the substrate is, the larger modulus values it gets; and the less thick the cell is , the larger modulus it estimates.

Another assumption is that the cell material is homogeneous and linear elastic, which is obviously controversial with the fact that cell is highly heterogeneous and the cell's modulus will increase as the deformation becomes larger. Depend on this invalid assumption, Hertz model neglects the material nonlinearity's contribution to the final nonlinearity of force-indentation curve.

In Hertz model, if the AFM tip is a sphere with radius R, the force on cantilever can be given by:

$$F(h) = \frac{4\sqrt{R}}{3} E^* h^{3/2} \qquad (2.1)$$

Where h is the indentation depth, E^* is the effective modulus of the tip-sample system which is given by:

$$\frac{1}{E^*} = \frac{1-\upsilon_{tip}^2}{E_{tip}} + \frac{1-\upsilon_{sample}^2}{E_{sample}} \qquad (2.2)$$

Where E_{tip} , υ_{tip} and E_{sample}, υ_{sample} are the Young's modulus and the Poisson ratios for the material of tip and sample, respectively.

From equation (2.1) and (2.2), we can see that the nonlinearity part in equation is $h^{3/2}$ which only corresponds to the indentation depth, which is in conflict with the fact that the nonlinearity of Force-Indentation curve comes from three parts: geometry nonlinearity, contact nonlinearity, material nonlinearity. So in this aspect, the application of Hertz model and Hertz-like model to estimate cell's elastic property is not that reliable.

2.3 CELL THICKNESS AND RADIUS' INFLUENCE ON THE EXPERIMENTAL FORCE-INDENTATION CURVE

Most cell elastic property characterization method only considers the cell materials' influence on the F-D curve, but the cell's thickness and radius also have large contributions to the measured curve. In this part, some simulation to show the cell thickness and radius's large influences on the F-D curve. Firstly, the cell material is chosen as one of estimated cell material which is fitted by a 3-order Ogden hyperelastic model. In the first group, the cell thickness is fixed as 8 um and the radius 6um, 8 um, 10 um, 12 um are simulated respectively to show the force-indentation curve difference with respect to radius; in the second group, the cell radius is fixed as 8 um and the height 6um, 8 um, 10 um and 12 um are simulated.

From Figure 6, the cell height's influence on the force-indentation is very obvious; with the same material and same indentation depth, the reaction of cell with height 6 um is almost 4 times of the reaction force of the cell with height 12 um. Fig 7 shows the differences between the reaction force between the simulated cell with same height and elastic property but with different cell radius. The characterization method which can capture the cell geometry's contribution to the F-D curve is desired to characterize the whole-cell elastic property.

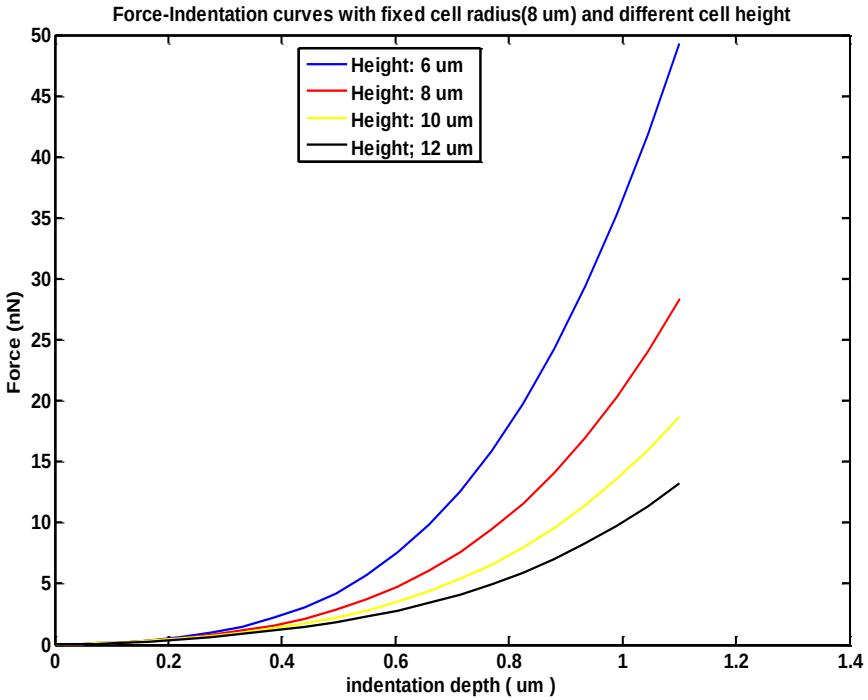

Figure 6. The cell height's influences on the force-indentation curve

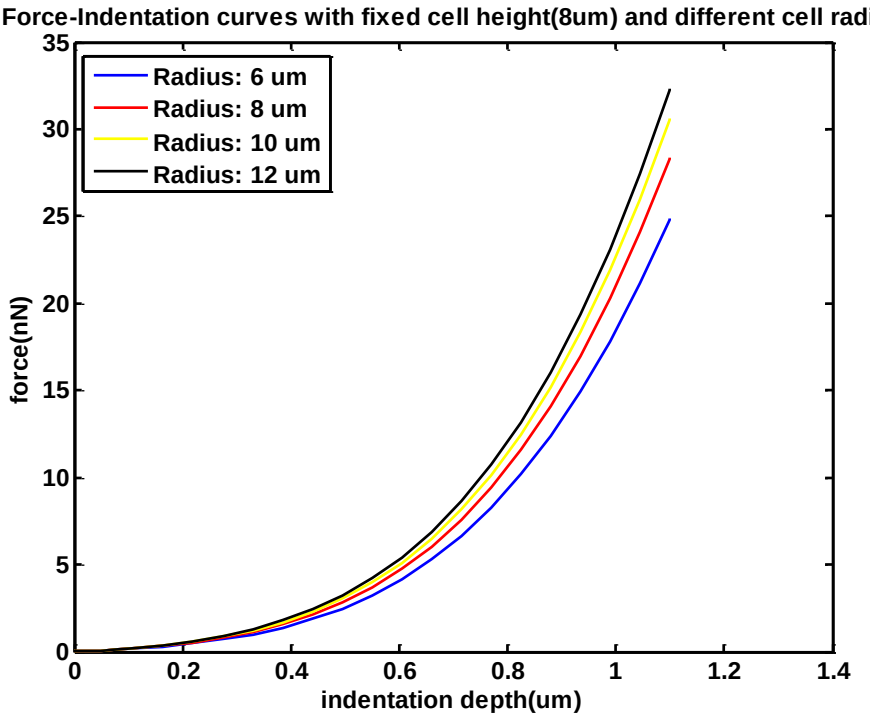

Figure 7. The cell radius's influences on the force-indentation curve

2.4 HYPERELASTIC MATERIAL MODEL AND ITS APPLICATION TO DESCRIBE THE CELL AND SOFT TISSUE MATERIALS

2.4.1 Hyperelastic model represented by strain energy density function

Hyperelastic model is a kind of constitutive model of ideally elastic material whose stress-strain relationship can be derived from the strain energy density function. The strain energy density function can be expressed in terms of the principal stretches λ_j , $j = 1,2,3$.

For example, Ogden model's strain energy density is written as:

$$W(\lambda_1, \lambda_2, \lambda_3) = \sum_{p=1}^{N} \frac{\mu_p}{\alpha_p} (\lambda_1{}^{\alpha_p} + \lambda_2{}^{\alpha_p} + \lambda_3{}^{\alpha_p} - 3) \qquad (2.3)$$

Where N is order of the model, μ_p and α_p are material constants. The principal stretches can be derived from the Right Cauchy-Green deformation tensor $\boldsymbol{C}$.

$$I_1{}^C := tr(C) = C_{II} = \lambda_1^2+\lambda_2^2+\lambda_3^2 \quad (2.4)$$

$$I_2{}^C := \frac{1}{2}[(trC)^2 - tr(C^2)]=\lambda_1^2\lambda_2^2+\lambda_2^2\lambda_3^2+\lambda_1^2\lambda_3^2 \quad (2.5)$$

$$I_3{}^C := \det C =\lambda_1^2\lambda_2^2\lambda_3^2 \quad (2.6)$$

And Green strain tensor **E** can be derived by

$$\boldsymbol{E} = \frac{\mathbf{1}}{\mathbf{2}}(\boldsymbol{C} - \boldsymbol{I}) \quad (2.7)$$

Where **I** is the identity matrix

The Cauchy Stress tensor σ is defined as

$$\sigma = \begin{bmatrix} \sigma_{xx} & \sigma_{xy} & \sigma_{xz} \\ \sigma_{yx} & \sigma_{yy} & \sigma_{yz} \\ \sigma_{zx} & \sigma_{zy} & \sigma_{zz} \end{bmatrix} \quad (2.8)$$

σ_{ij} are the nine components that completely define the state of stress in a point in the material.

Second Piola–Kirchhoff stress tensor is defined as $S = JF^{-1}\sigma F^{-T}$ whih can be derived from the strain energy density function by

$$S = \frac{\partial W}{\partial E} \quad (2.9)$$

By the strain energy density function and above equation, we can get the relationship between the stress and strain. Usually according to the stress-strain curve, we can fit the hyperelastic model.

The strain energy density is very powerful to describe a material, and different orders can apply to different situations. Usually 2 or 3 order Ogden material model can describe the soft tissue

or cell material very well. And other hyperelastic model such as the polynomial model also can describe the soft tissue and cell material.

2.4.2 **Whole-Cell elasticity's origin and its description by hyperelastic model**

Cell consists of very thin cell membrane, cytoplasm, cytoskeleton and the nuclei. The cytoskeleton contains three parts: microfilaments (actin filaments), intermediate filaments and microtubules. The thinnest filaments of the cytoskeleton are microfilaments, 3-6 nm in diameter and composed of actin protein, which are strongly related to the muscle contraction, cell gliding, contraction and cytokinesis. Intermediate filaments are about 5 nm in radius and responsible for the tensile strength for the cell. The scaffold of the whole cell are microtubules which are cylindrical tubes, 20-25 in diameter, and are related to cell organelles movement[20]. All these three components form the whole network of the cell, when subject to the external force, the force will transverse in the whole network and react to the external force [21, 22]. The cell cytoskeleton contributes to the cell's nonlinear elastic property, and many literatures have shown that soft tissues can be modeled by hyperelastic models, for example the Ogden hyperelastic model to model the biological tissues[23]. Ref [23] has shown that soft tissues' data can be fitted very well by the hyperelastic models while Hertz model can only fit it at small strain (less than 0.05), which directly shows the hyperelastic models' capabilities to equivalently describe the mechanical properties of biological tissue or cell.

By simulation and experiments, I also found that if we assume that cell is homogeneous, the hyperelastic model is suitable for describing the cell mechanical property. Several hyperelastic models has been used to describe the soft tissue and cell material property, for example in Ref [24] an eight- chain model is used to model the cell material, in Ref [25] a self-defined strain-energy

function is used to describe the soft tissues. And there are many currently available hyperelastic model, such as Mooney-Rivlin, Ogden, Polynomial, Yeoh, and Marlow. Different hyperelastic models are especially useful for different kinds of hyperelastic materials, for example, the Ogden material mode is used to describe the nonlinear stress-strain behavior of complex materials such as rubbers, polymers and biological tissues, which is developed by Ray W.Ogden in 1972. Because the similarity between cell and the soft tissue, the Ogden model is also very suitable for description of the cell materials.

2.5 FINITE ELEMENT ANALYSIS FOR CELL OR SOFT TISSUE MATERIAL CHARACTERIZATION

In the previous parts, Hertz model's limited ability to fit the experimental force-displacement curve has been shown; none of the Hertz model, exponential equation and the parallel-spring recruitment model considers the cell's geometry's influence on the final estimation of the cell elastic property. Another popular method to estimate the cell's nonlinear material property is finite element analysis. Finite element modeling of axisymmetric micro indentation tests has been used to measure the nonlinear elastic parameters of breast tissues, brain, liver and so on [17,24-28][3, 26-30]. In Ref [31, 32], the investigators used finite element modeling the AFM micro indentation of the fibroblasts and fungal hyphae to characterize their mechanical properties and measure the cell wall's elastic response during the cytoskeleton disassembly. In the following part, several groups' work to use the finite element method to estimate the cell elastic parameters will be shown.

T.Ohashi's group[33] firstly builds an axisymmetric finite element model and to simulate the AFM-indenting-Cell process, assuming that the cell material is homogeneous, isotropic and linear elastic material. The FEM model of the modeled rigid cantilever and linear elastic specimen is shown in Figure 8. The relationship between the applied force F and the resulting indentation depth δ is expressed in the following form (a and b parameters representing the nonlinearity and initial stiffness of the force-indentation curve)

$$F = a * \delta^2 + b * \delta \tag{2.10}$$

Let b' represent the linear coefficient of the simulation $F - D\ curve$. By comparison the simulation and experimental F-D curve, the FEM-based estimated Young's modulus E_{FEM} is obtained.

$$E_{FEM} = \frac{b}{b'} \tag{2.11}$$

The whole procedure of the estimation of E_{FEM} is shown in Figure 9.

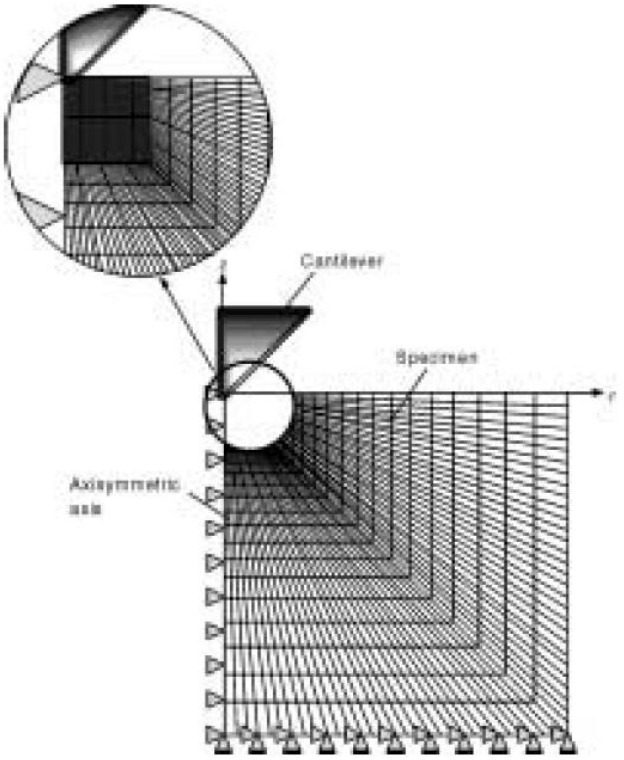

Figure 8. Axisymmetric finite element mesh from Ref [4].

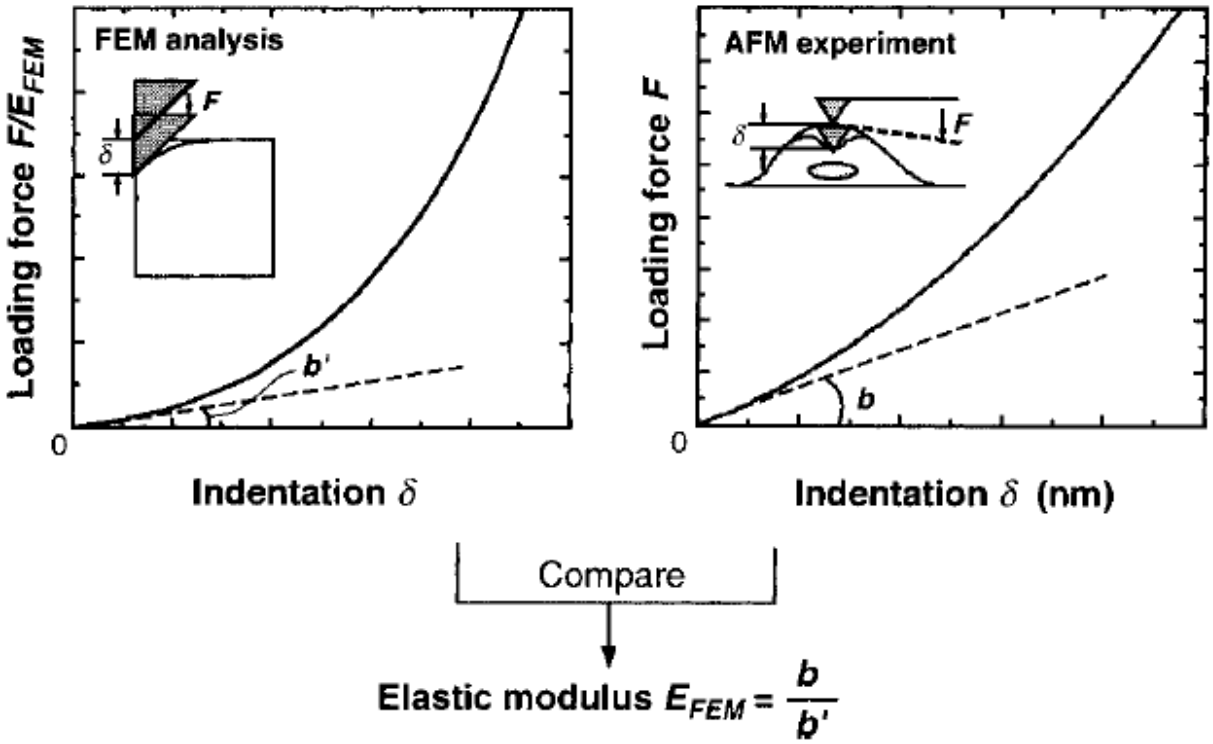

Figure 9.Estimation procedure of E_{FEM} [33]

Finite element method is used to estimate the Young's modulus of the cell by T.Ohashi's group. Although their results show better correlation with the experimental data, but the assumption that the cell material is linear elastic is still made and they derived E_{FEM} by single comparison between the experimental curve and simulated curve, so this method has limited capabilities to estimate the whole-cell elastic property.

The hyperelastic model which is expressed by the following strain-energy function is utilized by Martin Kauer [25] to model the soft tissue material.

$$W = \frac{\mu}{\gamma}\left(e^{\gamma(I_1-3)} - 1\right) + \alpha(I_2 - 3) \qquad (2.12)$$

Where γ and α are materials parameters, γ is in the exponential formulation and can capture different degrees of material nonlinearity. I_1 and I_2 represent the first and second invariant of the Deformation tensor respectively.

Then an axisymmetric finite element model is built to model the experiment setup; together with a Levenberg-Marquardt algorithm, the self-defined material model parameters are estimated by an inverse parameter determination process, which is shown in Figure 10.

This algorithm is powerful to describe the soft tissue's mechanical property by this self-define material model. But it still suffers several drawback; firstly, the choice of initial value is extremely important which can directly influence the convergence of the optimization process, but this algorithm does not give a good method to do this choice; secondly, the material model is fixed, for some other biological tissues or other materials, this model may not be able to describe their mechanical properties; thirdly, because each time of the optimization of these parameters, the algorithm will need one time of simulation, so the computation cost will be very large.

Inkyung Kang's group[24] takes use of an eight-chain model to model the cell material, which is given by the following formula:

$$\Psi = \mu_{8chain}\left[\frac{1}{2}(I_1 - 3) + \frac{1}{20\lambda_L^2}(I_1^2 - 9) + \frac{11}{1050\lambda_L^4}(I_1^3 - 27) + \frac{19}{7000\lambda_L^6}(I_1^4 - 81) + \frac{519}{673750\lambda_L^8}(I_1^5 - 243)\right] + \cdots \quad (2.13)$$

Where $\mu_{8chain} = shear\ moduli$; I_1=first invariant of the right Cauchy-Green strain tensor C, which is related to the Green-Lagrange strain tensor E as C=2E+I where I is the rank 2 unit tensor, and λ_L= distensibility or limiting network stretch. In this study, the five-term approximation of the eight-chain model is adopted.

In their algorithm, similarly an axisymmetric model is built and the sample material is assumed to be homogeneous and be suitable for this eight-chain material model. Then the material parameters including the thickness of the sample, shear modulus μ_{8chain} and limited network stretch in a range in certain interval are picked to do the finite element simulation, after the intensive simulation, a library of simulated force-indentation curves is formed. Then the experimental force-indentation curve is compared with the each force-indentation curve in the simulated library and then found the most similar one, the chosen simulated curve's corresponding material and thickness parameters are the estimated material model and thickness parameters. The whole estimation flow diagram is shown in Figure 11.

This algorithm is very easy to be implemented, but it suffers from two serious problems. Firstly, the parameters are specified in certain intervals; the estimated parameters resolution is relatively low, thus accurate estimation of the parameters cannot be obtained by finite computational cost; secondly, the computation cost of this algorithm is also very huge because of its method to traverse the parameters.

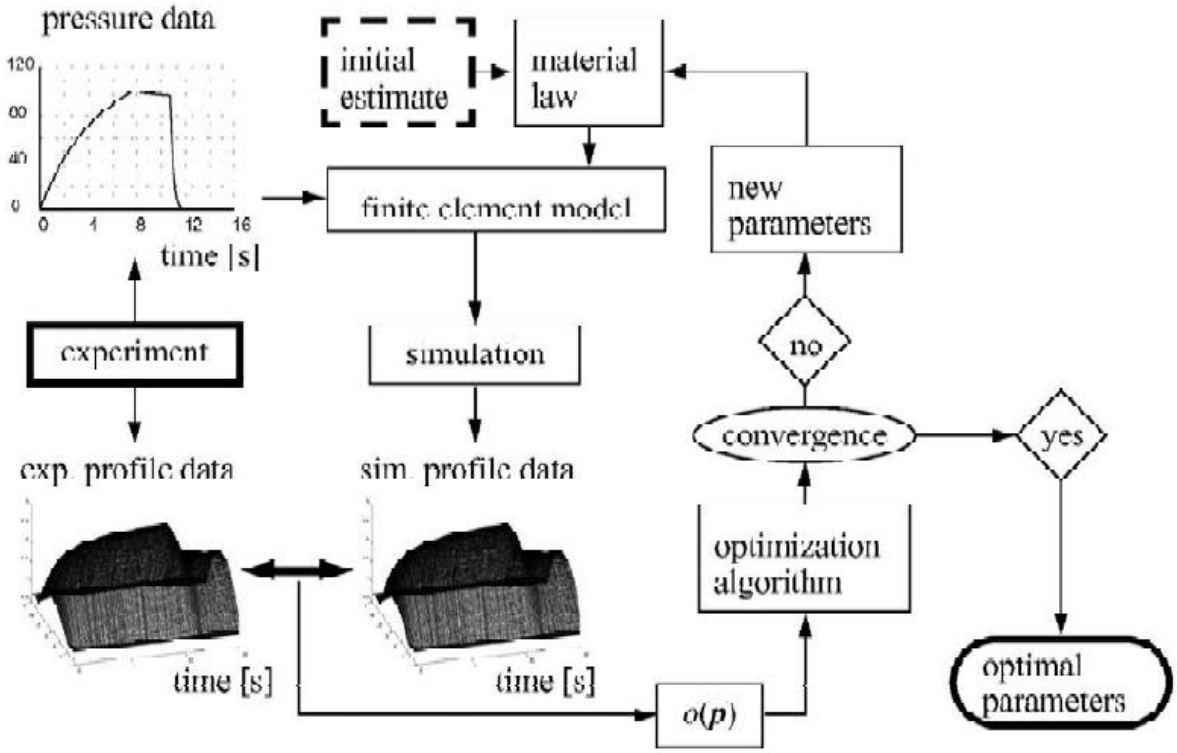

Figure 10. Material model parameter estimation process[25]

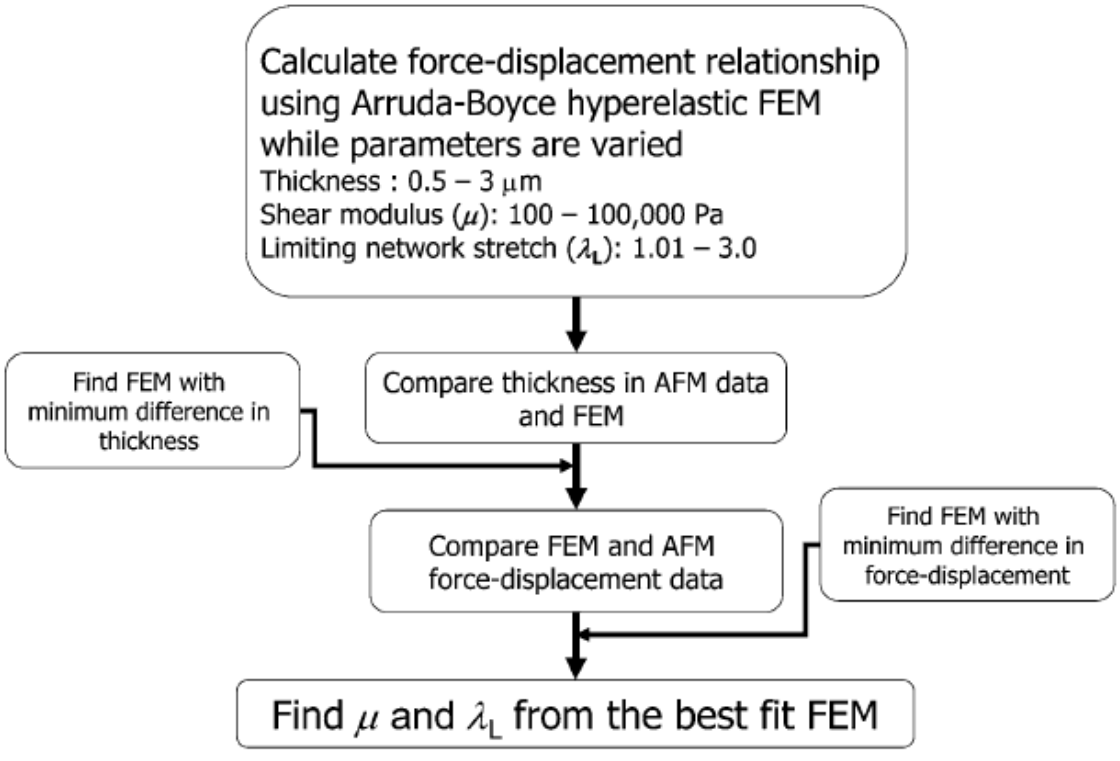

Figure 11. Flow diagram of the estimation of hyperelastic model parameters [24]

In conclusion, the Hertz model and its derivative model suffer from invalid assumption and can't handle geometry and material nonlinearity, and they can only measure the local elastic property. The large deformation and the material nonlinearity can be handled very well by finite element method. But according to the above discussion, almost all the above finite element methods (IFEM) suffer from huge computation cost which makes the FEM method less popular in the practical use than the Hertz model despite of its capability to handle the geometry and materials nonlinearity.

3.0 METHOD

3.1 BRIEF INTRODUCTION OF THE NEW FINITE ELEMENT ANALYSIS METHOD

In chapter 2, the Hertz model and the current available finite element method's capabilities to characterize the whole-cell mechanical property are discussed; different hyperelastic models and different material model parameters estimation methods are discussed. The huge computation cost and the limited capability to get a good enough match between simulated and experimental F-D curve make the finite element method less desirable. Here a new method which can overcome these drawbacks of the currently available FEM method is advanced. Firstly, based on the experimental F-D curve and cell and probe size information, one initial uniaxial stress-strain curve to represent the cell material is estimated. Then this estimated uniaxial stress-strain curve is fitted by a suitable hyperelastic model (usually Ogden hyperelastic model). Then fitted hyperelastic model parameters are used as the initial values for our finite element analysis to estimate the final uniaxial stress-strain curve (corresponding to certain hyperelastic model) which can represent the whole-cell elastic property. And similar to other FEM method, an axisymmetric finite element model is built to approximate probe-cell system, which can save huge amount of computation compared with the full 3D model. After each time of finite element simulation, simulated $F-D\ curve$ ($F_{FEM}(d)$ is extracted and compared with the experimental curve $F-$

$D\ curve$ ($F_{EXP}(d)$). Then the following rectification factor which is a function of indentation depth can be obtained:

$$w(d) = \frac{F_{EXP}(d)}{F_{FEM}(d)} \qquad (3.1)$$

The estimated uniaxial stress-strain curve is directly rectified by using above rectification factor to get the new estimated uniaxial stress-strain curve. This process is repeated until the difference between the simulated and experimental F-D curve becomes small enough (below 5% is easy to be achieved); the final estimated uniaxial stress-strain curve is the estimated result; this estimation process is very fast, only several times of simulation are needed to get satisfied match between the simulation and experimental F-D curve. The estimation process is similar to the proportional gain control, which guarantees the quick convergence of our algorithm.

3.2 MEASUREMENT OF CELL THICKNESS AND DIAMETER

Our algorithm assumes that a sphere probe is used to indent the cell on a very flat substrate which is similar with that shown in Figure 12a and Figure 12b. The size of the sphere probe may vary from several micrometers to about 20 um. Here the method of measurement of the cell thickness and diameter is designed according to Veeco Dimension 3100 AFM system, in other AFM system, the method may be different. The cell's diameter is measured by AFM's stage motors and CCD camera. In the beginning, the vertical line in CCD camera view is made to be tangential to the left side of the cell by moving the AFM stage shown in Figure 12c, recording the stage's x coordinate (X_1 um) at this position; then AFM stage is moved to make the vertical line to be tangential to the cell's right side shown in Figure 12d, recording the x coordinate again (X_2 um); finally the cell's diameter is obtained by the difference of the two coordinates, $|X_2 - X_1|$.

Cell's thickness is measured by recording the piezoceramics' position in the Z direction. Firstly, AFM approaches the blank substrate, when the tip contacts the substrate, the coordinate in Z direction (Z_1 um) is recorded; then the tip is withdrawn and moved to be above the cell; then let the tip approach the cell surface, when tip contacts the cell surface, the coordinate is recorded (Z_2 um), finally the cell's thickness τ is obtained by the difference of the two Z positions $| Z_1 - Z_2 |$.

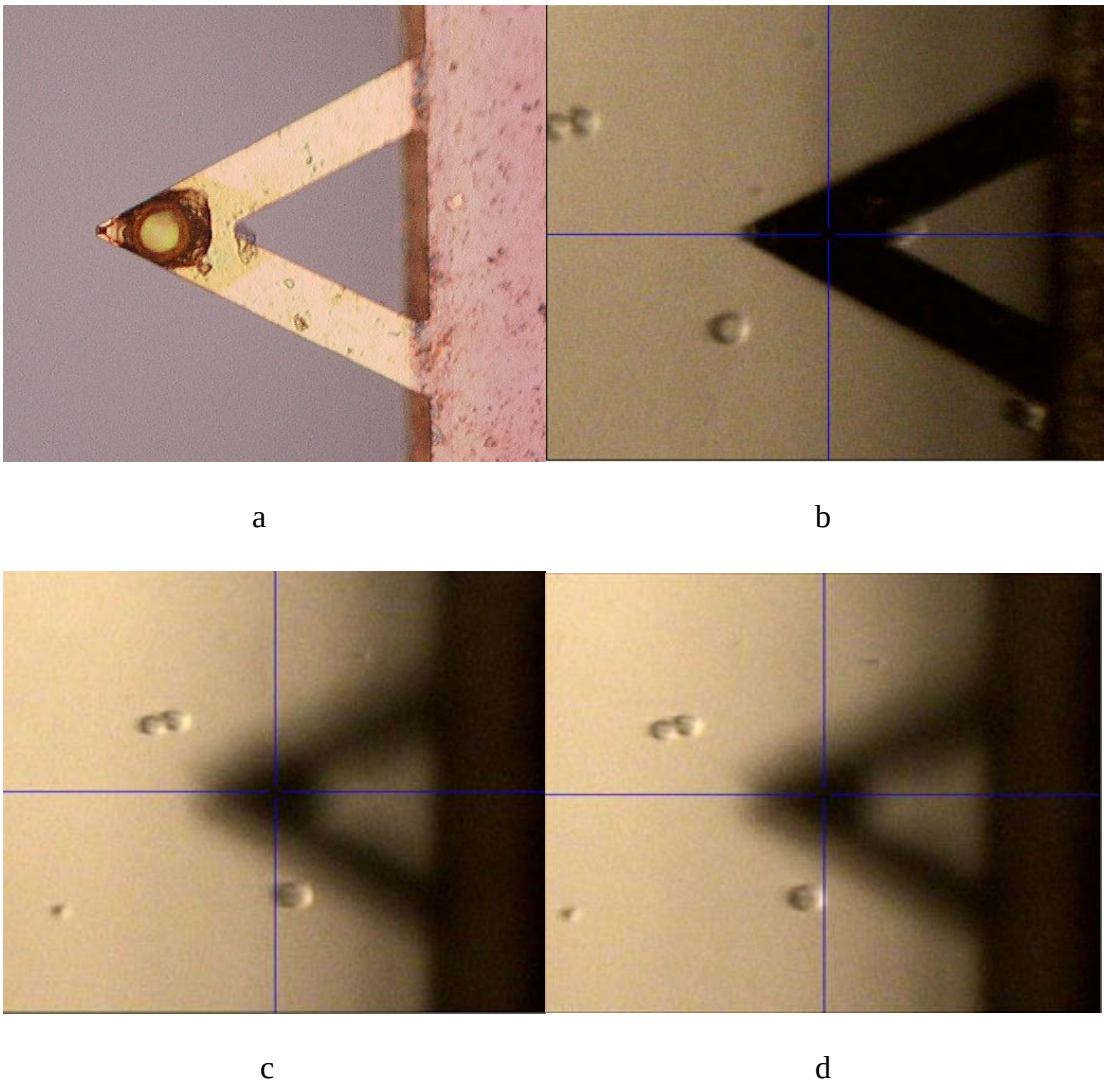

a b

c d

Figure 12: Measurement of cell's thickness and diameter by AFM stepper-motors. (a) Sphere probe; (b) Cells and probe; (c) Vertical line tangential to the left side of the cell. (d) Vertical line tangential to the right side of the same cell.

3.3 PREPROCESSING THE RAW DATA

The raw data we get from the Veeco Dimension 3100 System is cantilever deflection(u) versus cantilever base extension(z) curve, $u{\sim}z$ curve. Three steps need to be done in this preprocessing step; the first is to determine the contact point between the AFM tip and the cell surface; the second one is to transform $u{\sim}z$ curve into $F-D\ curve$; the third one is to estimate the initial stress-strain curve from the $F-D\ curve$.

3.3.1 Determination of contact point

The raw $u{\sim}z$ curve is firstly smoothed by moving-average method to remove the large disturbance caused by noise. Before the AFM tip contacting cell surface, the change of the cantilever deflection can be only caused by noise, so the cantilever deflection u will not be monotonically changing with increase of cantilever base extension before contact; but after contacting the cell surface, the cantilever deflection will definitely increase with the increase of the cantilever base extension, so we can determine the contact point by finding the point after which the deflection monotonically increases with the increase of cantilever base extension z.

3.3.2 Derivation of $F-D\ curve$ from $u{\sim}z$ curve

By the cantilever base extension $z=u+d,\ \ d$ is the indentation depth, the indentation depth can be obtained by $d=z-u$. Then the force F can be got by $F=k*u$, k is the cantilever's spring constant. Finally the F-D curve is derived from u~z curve.

3.3.3 Estimation of initial stress-strain curve

In this estimation method, the available information are cell shape and size, AFM tip shape and size, F-D curve. The tip is assumed to be a sphere with radius R, the thickness of the cell is τ. According to the Hertz model, a sphere with radius R indenting an elastic half-space to the depth d will create a contact area:

$$A = \pi(\sqrt{Rd})^2 = \pi Rd \tag{3.2}$$

The nominal uniaxial stress can be estimated to be:

$$\sigma = \frac{F}{A} = \frac{F}{\pi Rd} \tag{3.3}$$

The nominal uniaxial strain can be estimated to be:

$$\varepsilon = -\frac{d}{\tau} \tag{3.4}$$

Then the F-D curve is transformed into the initial stress-strain curve by the above three equations. Although the contact area is estimated based on Hertz model and the strain is also approximated, the approximation is good enough to be treated as the initial value to further estimate the accurate uniaxial stress-strain curve, which can be regarded as the equivalent cell elastic property.

Another aspect is that here the acquired uniaxial stress-strain curve $\sigma(\varepsilon)$ in this step is not smooth. Several methods can be applied to smooth it, for example, hyperelastic models can be used to fit $\sigma(\varepsilon)$; splines can also be utilized to smooth the stress-strain curve.

3.4 FINITE ELEMENT MODELING OF AFM-INDENTING-CELL SYSTEM

3.4.1 Geometry modeling

The sphere tip indenting cell system is modeled by an axisymmetric finite element system and the probe is modeled as a rigid body while cell modeled as deformable because probe is far more rigid than cell. The cell is modeled as a sphere cap or the complementary part of the sphere cap, the model should have the same diameter and thickness with the experimental measured diameter and thickness. The bottom boundary of the cell model is fixed; the displacement is applied to the reference point of the rigid probe in y direction and the x direction of the probe is fixed, which is shown in Figure 13. Large enough mesh size with which the simulation results are less 1% different from the one with much smaller mesh size is adopted in the simulation in order to achieve enough simulation accuracy and reduce the computation cost to largest extent. Total reaction force on the cell bottom boundary is collected to form the F-D curve.

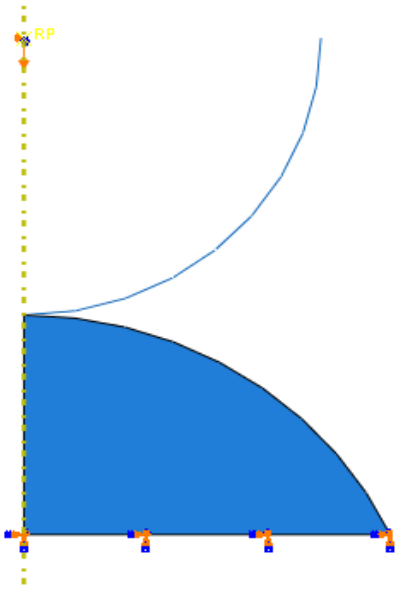

Figure 13: Finite element modeling of the probe-cell system

3.4.2 **Modeling Process in FEM software**

The FEM software Abaqus 6.10(used to be product of Abaqus Inc, which has been acquired by Dassault Systems, especially good for contact analysis) is used in this algorithm. The geometry modeling is done as mentioned in Geometry modeling part in the first step and then the initial stress-strain curve estimated by equation (3.2~3.4) is imported into the Material Evaluate module of the Abaqus, then hyperelastic models are chosen to fit this uniaxial stress-strain curve by Abaqus, the one which can fit the initial curve best and has the best stability are chosen as the hyperelastic model used to estimate the cell's elastic property. Then the simulation is run and the reaction force on the cell bottom are collected to form the Force indentation curve. The work in FEM software are three major steps, the first is to fit the initial estimated or rectified uniaxial stress-strain curve during the estimation process by the chosen hyperelastic model in the Material Evaluate module of the software, the second step is to run the simulation and the last step is to collect the reaction force on the cell bottom to form the force indentation curve. The whole three steps can be described by the Abaqus script, so we do not need to interrupt the estimation process, everything is done in one step by well-prepared Abaqus script in Python programming language. The detailed estimation process is shown in the next part "Estimation of Cell Elastic Property".

3.5 ESTIMATION OF CELL ELASTIC PROPERTY

In Hertz model, only one parameter is used to represent the cell material property. Here it is assumed that the cell's material property can be described by a hyperelastic model, which is a very general method to show the change of elastic modulus with the increase of strain. Firstly we have to understand the relationship between the corresponding hyperelastic models's uniaxial $\sigma - \varepsilon\ curve$ and the corresponding $F - D\ curve$. The simplex system similar to our system is a spring; firstly we have an initial spring constant k', then we simulate pressing the spring by this initial value and obtain the simulated $F' - D'\ curve$. By comparing the difference of the slope of the simulated $F' - D'\ curve$ and experimental $F - D\ curve$, we can get the real spring constant $k = k' * \frac{k}{k'}$. The above method seems to be unnecessary because we can get the spring constant k by only one experiment $F - D\ curve$, $k = \frac{F}{D}$. But for the estimation of the nonlinear elastic property of a complex system, for example, our probe-indenting-cell system, the similar process will be very useful and necessary. For our case, only from one $F - D\ curve$, the uniaxial stress-strain curve which can represent the elastic property can never be obtained by one calculation because this $F - D\ curve$ contains much more information than the spring case, such as the probe shape and size, cell shape and size, the cell's nonlinear elastic material property, the substrate's property; So the finite element modeling is needed to cover all the available information. The stress means the force in unit area and the strain means the normalized measurement of the deformation or displacement here; so the trend is the same for the $F - D\ curve$ and uniaxial $\sigma - \varepsilon\ curve$ although no exact relationship can be derived because of the complicated system. The larger the elastic moduli at the current strain, the higher the slope value of the stress-strain curve are at the

same strain. So we can recursively rectify the $\sigma - \varepsilon\ curve$ to approach the real uniaxial stress-strain curve according to the difference between the simulated and experimental $F - D\ curve$.

Let $\sigma^i(\varepsilon)$ denote the estimated uniaxial stress-strain curve, i represents the ith simulation and $\sigma^1(\varepsilon)$ is the initial estimation of stress-strain curve. $F_{FEM}^i(d)$ Denotes the force-indentation curve obtained from ith simulation and $F_{EXP}(d)$ is the experimental $F - D\ curve$; and $w^i(d)$ is rectification factor in ith recursive step.

$$w^i(d) = \frac{F_{EXP}(d)}{F_{FEM}^i(d)} \tag{3.5}$$

$$\sigma^{i+1}(\varepsilon) = \sigma^i(\varepsilon) * w^i(\varepsilon * \tau) \tag{3.6}$$

The new $\sigma - \varepsilon\ curve$ obtained from equation (3.6) may not be very smooth. A stable hyperelastic model (usually Polynomial or Ogden hyperelastic model) is adopted to fit the new $\sigma - \varepsilon\ curve$ and the uniaxial stress-strain curve from this fitted model is utilized in the next step's simulation. Then the rectified $\sigma - \varepsilon\ curve$ from last step is used in the new step's FEM simulation and then rectified by the simulation results until satisfied match between the experimental and simulated $F - D\ curve$ is reached. The match error rate between the experimental and simulated $F - D\ curve$ is calculated by

$$err^i = \frac{||F_{EXP}(d) - F_{FEM}^i(d)||}{||F_{EXP}(d)||} \tag{3.7}$$

Usually this process is very fast. When estimated $\sigma - \varepsilon\ curve$ is far from the real one that can represent the cell material property, the simulated $F - D\ curve$ is also far from the experimental $F - D\ curve$; Then the resulted rectification factor will be relatively large and make the current estimation move much closer to the real one in next step. The process of adjusting the uniaxial stress-strain curve based on the difference between the simulated and experimental $F - D\ curve$ is just like the feedback in the control system. Firstly it is coarse adjustment, which makes

the current value move to the objective value quickly; then it is fine adjustment, which is more slowly and moves the current value even closer to the objective values. This is why our method is very fast and accurate. The whole process is shown as a flowchart form in Figure 15.

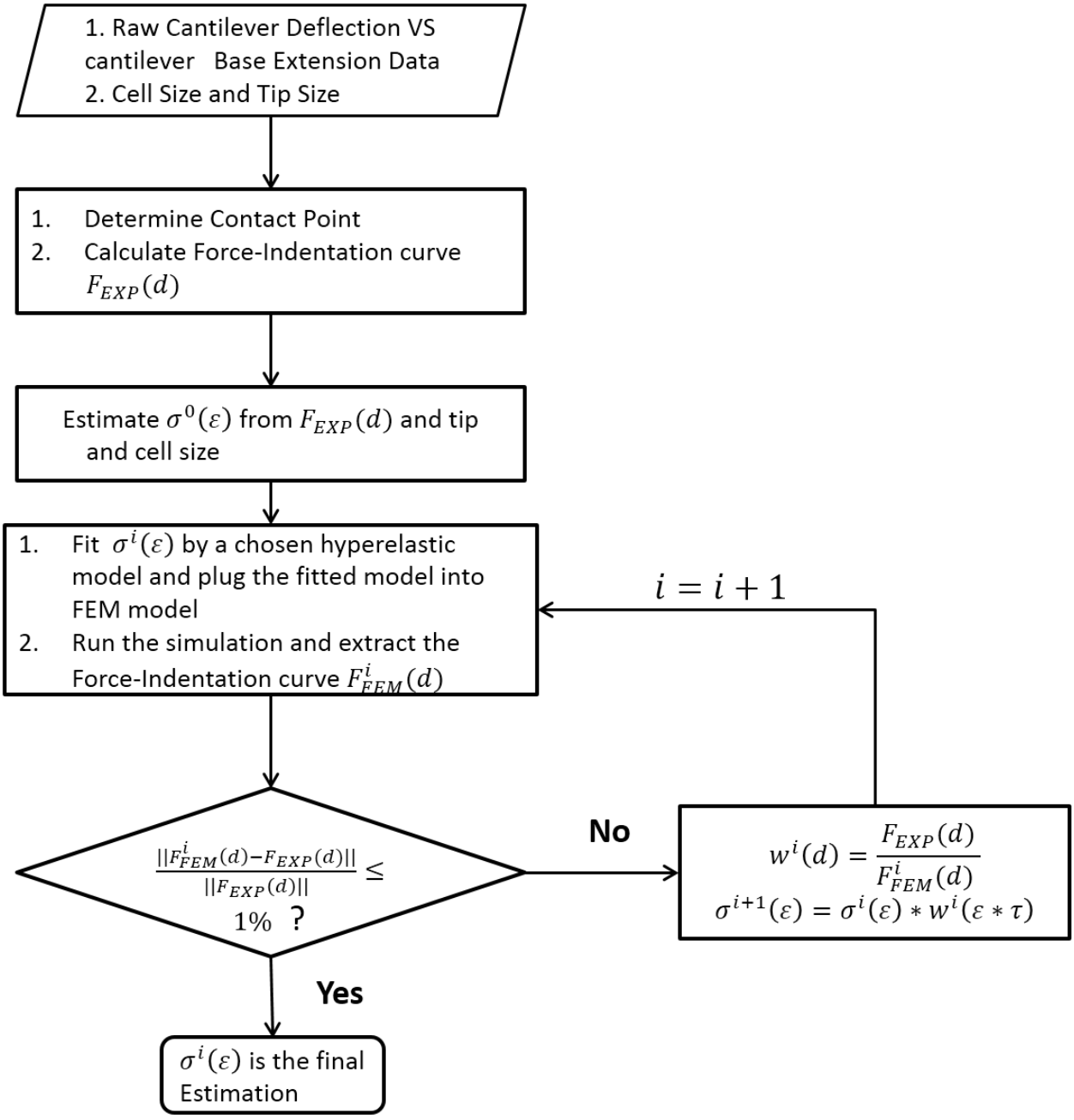

Figure 14. Flowchart of cell elastic property estimation by fast inverse finite element analysis

4.0 EXPERIMENTS AND DISCUSSION

4.1 ESTIMATION OF UNIAXIAL STRESS-STRAIN CURVE BY FINITE ELEMENT ANALYSIS IN EXPERIMENTS

In this experiment, the force-indentation curve on SH SY5Y cell is obtained, the cell's diameter is about 19 um and the height is about 7 um. The cantilever deflection VS cantilever base displacement curve is shown in Figure 15a. Then the derivative of the deflection is calculated to find the contact point shown in Figure 15b. By the contact point, the raw data is transformed into a force-indentation curve shown in Figure 15c. Consider cell's size and probe's size, we obtain the initial estimation of uniaxial stress-strain curve shown in Figure 15d.

After preprocessing the raw data, an axisymmetric model is built and the initial estimated uniaxial stress-strain used as the initial material. Then a Python script is written by use of the functions in Abaqus script library; the script is ran in Abaqus 6.10 to recursively rectify the estimated uniaxial stress-strain curve until the satisfied match (usually higher than 95%) is achieved. After indentation 2.2 um, the stress in vertical direction is shown in Figure 16a (the color from deep blue to deep red representing the stress from maximum to minimum). From the distribution of stress, we can directly see that the bottom has large influence on the stress

distribution and then affects the reaction force on the tip. Finite element analysis can capture the bottom influence, while the original Hertz model definitely cannot do it. Even some modified Hertz model tried to consider this problem, the analytical formula cannot do as well as the direct simulation[16]. The Abaqus simulation is run recursively to fit the experimental F-D curve; the fitting process in our algorithm is shown in Fig 16b; only 6 times of simulation is consumed to reach more than 99% match between the simulation and experimental force-indentation curve. The Hertz model fitting of experimental curve is also shown in this figure, because of many invalid assumption of Hertz model, the fitting accuracy is very low. Our fitting process is pretty fast compared to the current available finite element analysis algorithms shown in the previous part. From Fig 16b, we can see that initially the force-indentation curve of the 1st simulation(green curve) is far away from the experimental curve(red one); because of this large difference, the uniaxial stress-strain curve is adjusted to a large extend; then the gray curve move a big step to become closer to the experimental one. Flowingly, the curve moves finely to try to fit the experimental one accurately. The whole rectification process is just like a proportional control process, large error will result in large adjustment; the initial large adjustment resulted from the large initial error; then as the error becomes smaller and smaller, the adjustment is becoming finer and finer. The error decreasing process is shown in Figure 16d. This unique mechanism of this algorithm ensures its fast and fine fitting of simulation force-indentation curve to the experimental curve.

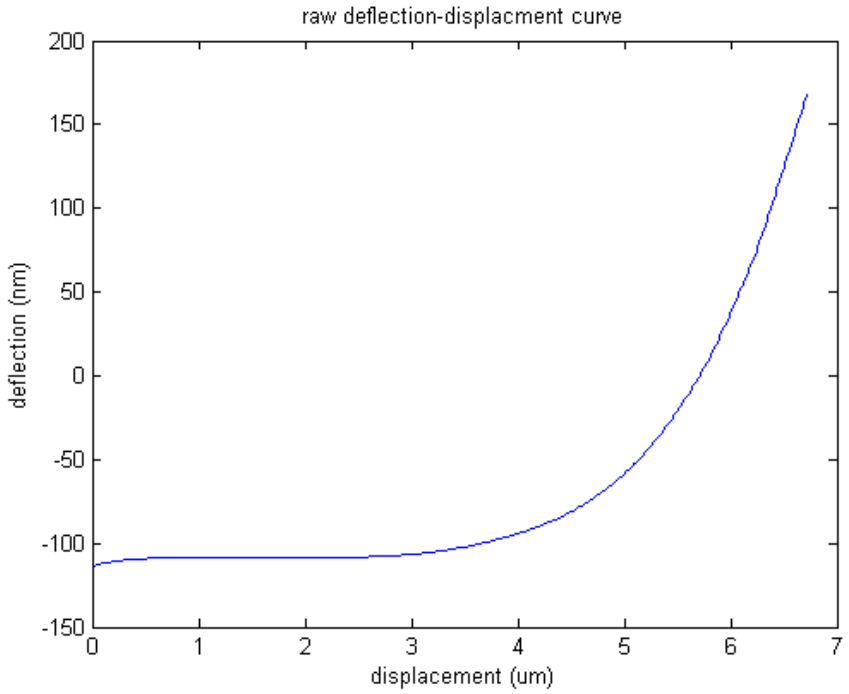
raw deflection-displacment curve
deflection (nm)
displacement (um)
200
150
100
50
0
-50
-100
-150
0
1
2
3
4
5
6
7

a

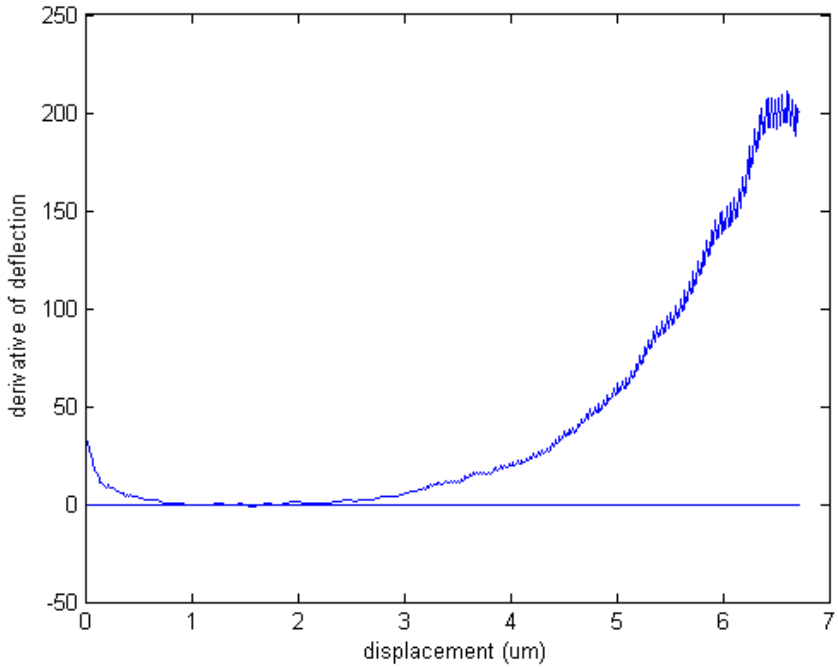
derivative of deflection
displacement (um)
250
200
150
100
50
0
-50
0
1
2
3
4
5
6
7

b

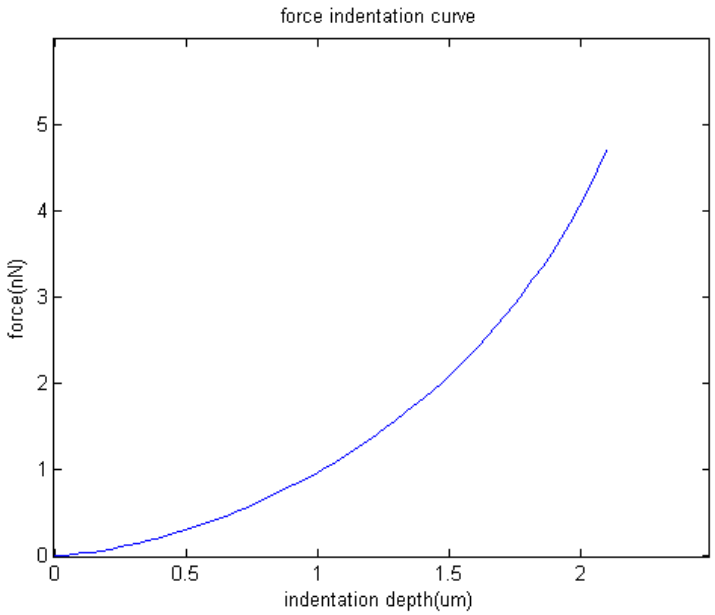

c

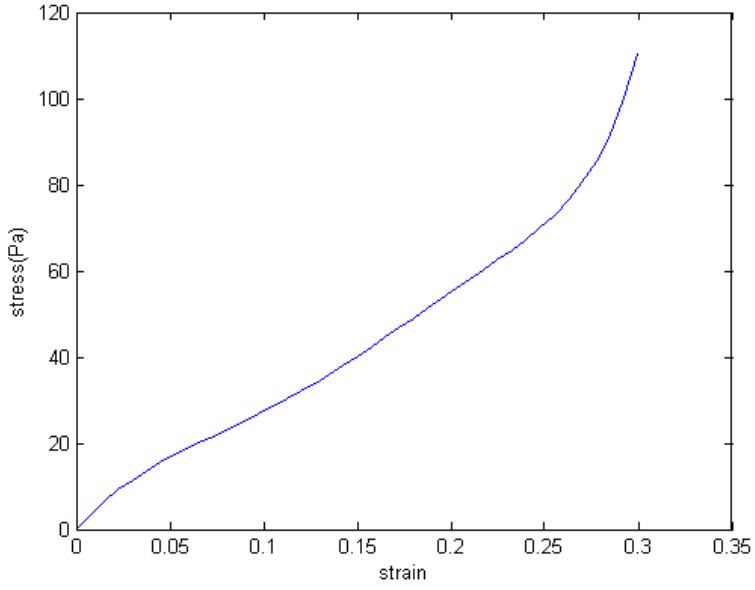

d

Figure 15. Preprocessing the raw data from AFM system. (a) Raw deflection-displacement curve. (b) Determination of contact point by derivation of deflection. (c) Derived experimental force-indentation curve. (d) Initial estimated uniaxial stress-strain curve.

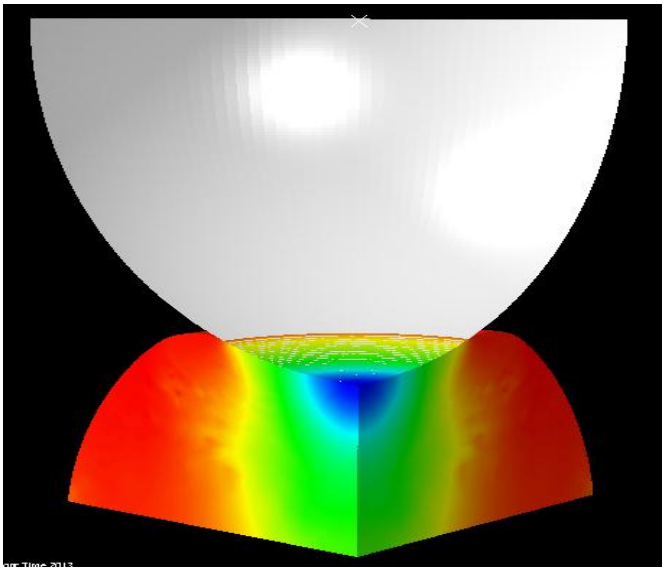

a

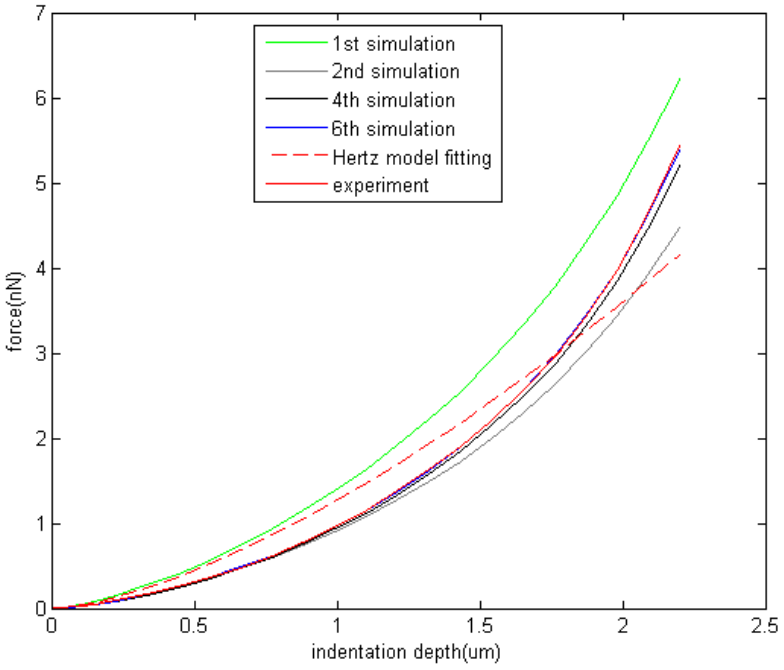
1st simulation
2nd simulation
4th simulation
6th simulation
Hertz model fitting
experiment
force(nN)
indentation depth(um)
0
1
2
3
4
5
6
7
0
0.5
1
1.5
2
2.5

b

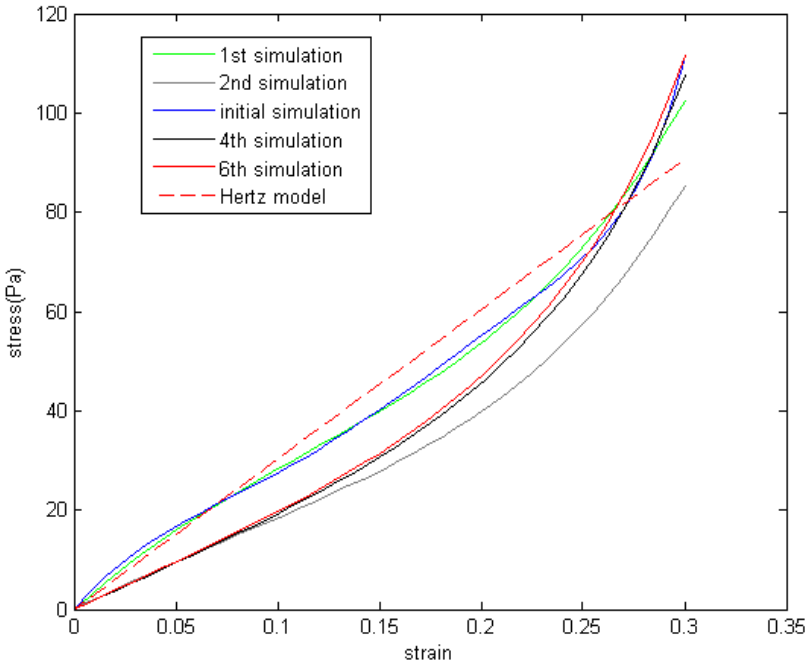
1st simulation
2nd simulation
initial simulation
4th simulation
6th simulation
Hertz model
stress(Pa)
strain
0
20
40
60
80
100
120
0
0.05
0.1
0.15
0.2
0.25
0.3
0.35

c

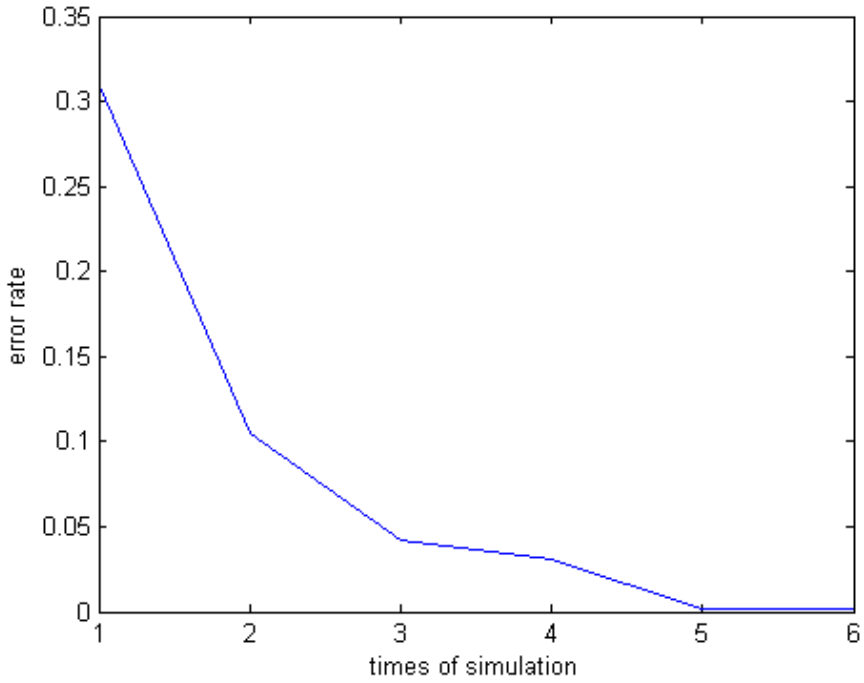
error rate
times of simulation
0
0.05
0.1
0.15
0.2
0.25
0.3
0.35
1
2
3
4
5
6

d

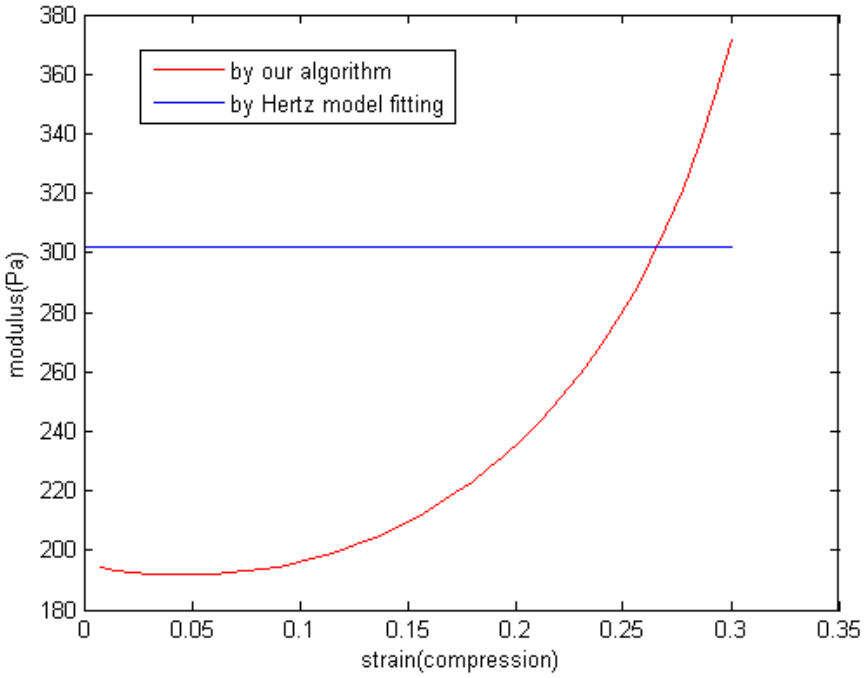

e

Figure 16. Estimation of uniaxial stress-strain curve by finite element analysis. (a) Stress distribution in Y direction. (b) Fitting process of simulation force-indentation curve to the experimental one. (c) Corresponding uniaxial stress-strain curve. (d) Self-defined modulus (uniaxial stress / strain). (e) Error rate of the simulation force-indentation curve decreasing with increase of simulation times.

The evolution of estimated uniaxial stress-strain curve is shown in Figure 16c, the blue curve is the initial uniaxial stress-strain curve and the red curve is from the final simulation, and it is also the final estimated result. During the simulation process, the rectified uniaxial stress-strain curve is fitted by 2-order Ogden hyperelastic model, then the fitted material model is used in the next simulation and rectification step. A hyperelastic model should be chosen in the Abaqus software, it cannot run only with the uniaxial stress-strain curve. And Ogden model is designed

to describe the biological tissue, it also do very well to describe the equivalent cell material. Of course, other materials model can also be used, for example polynomial model.

We define the modulus as $E(\varepsilon) = \frac{\sigma}{\varepsilon}$; as the strain varies from 0 to -0.3, the elastic moduls increases from 194 Pa to 371 Pa shown in Fig 16e; meanwhile the Hertz model fitting only gives a single number 302 Pa. Our algorithm successfully capture cell's nonlinear material property while the Hertz model cannot do it.

4.2 DISCUSSION

4.2.1 Experiments on different cells

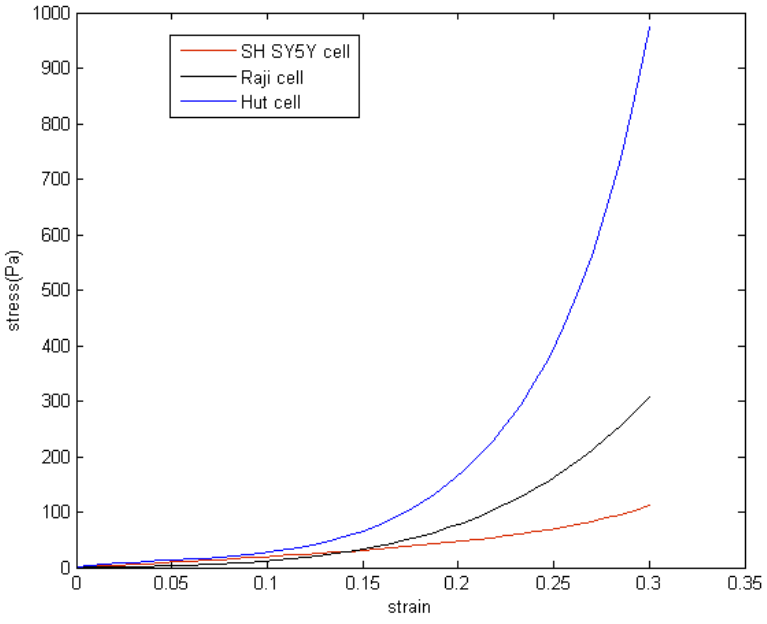

Figure 17. Comparison of estimated uniaxial stress-strain curve of different kinds of cells

We measure the force-indentation curves on different cells surface; the first one is SH SY5Y cell with diameter 19 um and height 7 um, the second one is Raji cell with diameter 22 um and height 7.1 um, and the one is Hut cell with diameter 16 um and height 10 um. The estimated uniaxial stress-strain curves of these three cells by our algorithm is shown in Figure 17. From Figure 17, we can clearly see that when the strain is in the range 0~0.1, there are not big differences between these three curves, while when the strain is larger than 0.15, it is crystal clear that Hut cell is the stiffest among the three and SH SY5Y cell is softer than the Raji cell. If the SH SY5Y cell and Raji cell are compared in the whole strain range, in the small strain, SH SY5Y cell is stiffer than the Raji cell, while in the large strain it is softer than the Raji cell. So by this comparison, we at least can get the conclusion that the cell material is highly nonlinear, the single Young's modulus estimated in the small strain range cannot reveal the full elastic property of the cell. The finite element analysis method can take use of the cell and probe information to build an axisymmetric model and the cell material's nonlinearity property is also covered. Since the whole cell elastic property should be compared in a large strain range, this improved application of finite element analysis to the estimation of the uniaxial stress-strain estimation of the cell material is desired. But this result cannot give the conclusion that all Hut cells are stiffer than the Raji cells because the cell's conditions also affect its elastic property a lot; so a solid conclusion about the whole-cell elastic property of different kinds of cells should also be based on the cell conditions.

4.2.2 **Comparison with other inverse finite element methods**

The successful utilization of available information and the design of a proportional-gain feedback method make our method convergent very quickly. In Ref [25], an optimization method is taken use of to estimate the material model's parameters, firstly the number of model parameters has to be restricted to a small number because each parameter will construct one dimension of the optimization space, too many parameters will make the optimization hard to converge; even though it can converge, the computational cost will be too huge, so they have to choose the material model with as less parameters as possible. In their algorithms, every time of updating the optimization objective function, a complete simulation has to be conducted, so the speed in searching optimal parameters in parameters space is very slow; compared with this algorithm, our algorithm directly rectify the whole uniaxial stress-strain curve which will search in the high-dimension parameters space, so each time of optimization is more efficient and the increase the complexity of the material model will not affect the optimization process. Another example is in Ref [24], the material parameters are chosen in certain reasonable range and then uniformly sample certain number of parameters in this range, finally these parameters are used in the simulation to build an F-D curve library, each of the F-D curves in the library corresponds to different model parameters. The experimental F-D curve is compared with each one in this F-D curve library, the one with the minimum difference with the experimental data is chosen, and then its corresponding material parameters is considered as the estimated material parameters. This method is more coarse than the algorithm shown in Ref [25]; in order to get fine estimated results, its F-D curve library has to be large enough, so the computational cost will be too expensive. The method in Ref [24] is to transverse the whole parameter space, while the method in Ref [25] is to use an optimization

algorithm to search in the parameter space. In contrast, our algorithm is to take use of physical properties to avoid the parameter space searching, which saves huge computational cost.

4.2.3 **Discussion of the possible estimation error by this algorithm**

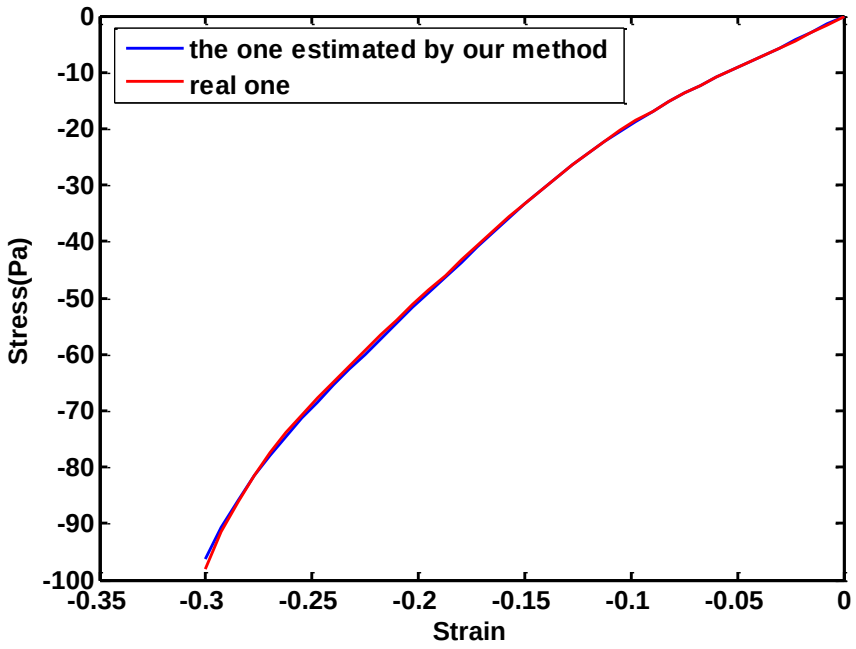

Figure 18. Comparison of the estimated stress-strain curve and the real curve (corresponding to 2-order Polynomial hyperelastic model)

In this part, a simulation experiment is done to demonstrate the unique solution of this algorithm. Firstly, we build a model of rigid probe indenting cell, cell's material is chosen as the one whose uniaxial stress-strain(2-order Polynomial hyperelastic model) is shown in the red curve of Figure 18, then we run the simulation and its Force-Displacement curve is obtained. By this calculated Force-Displacement curve and our algorithm, the material corresponding to this Force-Displacement curve is estimated. Finally, the estimated material parameters with the real material

parameters is compared and shown in Figure 18. From this comparison, It is clear that the uniaxial stress-strain curve can be accurately estimated by our algorithm from the F-D curve.

But this perfect estimation is based on the perfect setup, firstly the material model in this simulation is homogeneous and assumed to be known, but in reality, the cell's material model is heterogeneous and unknown; secondly the cell size in the simulation is completely known, but in experiments, the cell size cannot be accurately measured and in my algorithm the cell shape is approximated by axisymmetric model. All these difference between the assumptions and the real experiments will result in the estimation errors, but these errors has been reduced to a large extent compared to the current available methods in characterizing the cell materials.

5.0 CONCLUSION

In this thesis, a new method to estimate the whole-cell elastic property is advanced. This method reduces the computational cost to a large extent compared with current inverse finite element analysis methods. Our method can use any suitable hyperelastic model to describe the cell material property; because different cells may have to be described by different material model, choice of specific fixed material model can't apply to all situations. In other inverse finite element method, one hyperelastic model is adopted and then an optimal search algorithm is used to search for a satisfied set of material model parameters which can make the simulation and experimental $F - D\ curve$ match to certain satisfied extend; however, the search algorithm is usually blind and the search process requires a lot of times of FEM simulation, which will cost a lot of time, so the current finite element method is usually very slow and time consuming and thus not very feasible. Another problem is that after fixing a hyperelastic model, this model may have stability range, which may make it not suitable to describe the cell property. But our new method firstly gives a reasonable initial value and then uses the feedback-like algorithm to rectify the whole stress-strain curve, which is very efficient. Only a few times of simulation are needed for achieving the satisfied match; and then the FEM simulation process is optimized, the mesh size which ensure the less than 1% simulation error is chosen to minimize the computational cost. The main reason why our new method can work so fast and give better results than others is that we are taking use of more available information than others in the whole estimation process. For this kind of inverse problem,

more available information that can be incorporated into the estimation process, better results we can get.

Currently, standard available hyperelastic models are adopted to characterize cells' mechanical properties. A better self-designed hyperelastic model may make this algorithm's convergence faster and the description of the cell mechanical properties more reasonable.

BIBLIOGRAPHY

[1] A. Tajaddini, D. L. Kilpatrick, and D. G. Vince, "A novel experimental method to estimate stress-strain behavior of intact coronary arteries using intravascular ultrasound (IVUS)," *Journal of Biomechanical Engineering-Transactions of the Asme*, vol. 125, pp. 120-123, Feb 2003.

[2] D. Kilpatrick, C. P. Xu, R. Vito, and S. Glagov, "Correlation of Mechanical Behavior and Mmp-1 Presence in Human Atherosclerotic Plaque," *Journal of Mechanics in Medicine and Biology*, vol. 2, pp. 1-7, Mar 2002.

[3] A. Samani and D. Plewes, "A method to measure the hyperelastic parameters of ex vivo breast tissue samples," *Physics in Medicine and Biology*, vol. 49, pp. 4395-4405, Sep 21 2004.

[4] T. A. Krouskop, T. M. Wheeler, F. Kallel, B. S. Garra, and T. Hall, "Elastic moduli of breast and prostate tissues under compression," *Ultrasonic Imaging*, vol. 20, pp. 260-274, Oct 1998.

[5] Q. S. Li, G. Y. H. Lee, C. N. Ong, and C. T. Lim, "AFM indentation study of breast cancer cells," *Biochemical and Biophysical Research Communications*, vol. 374, pp. 609-613, Oct 3 2008.

[6] M. Lekka, K. Pogoda, J. Gostek, O. Klymenko, S. Prauzner-Bechcicki, J. Wiltowska-Zuber, *et al.*, "Cancer cell recognition - Mechanical phenotype," *Micron*, vol. 43, pp. 1259-1266, Dec 2012.

[7] M. Lekka and P. Laidler, "Applicability of AFM in cancer detection," *Nature Nanotechnology*, vol. 4, pp. 72-72, Feb 2009.

[8] B. Cappella and G. Dietler, "Force-distance curves by atomic force microscopy," *Surface Science Reports*, vol. 34, pp. 1-+, 1999.

[9] K. G. Arantxa Vilalta-Clemente, "Principles of Atomic Force Microscopy," *Physics of Advanced Materials Winter School*, 2008.

[10] *http://www.nanoscience.com/products/afm_tips.html*.

[11] *http://www.nanoandmore.com/AFM-Probe-CP-NCH-Au.html*.

[12] T. G. Kuznetsova, M. N. Starodubtseva, N. I. Yegorenkov, S. A. Chizhik, and R. I. Zhdanov, "Atomic force microscopy probing of cell elasticity," *Micron,* vol. 38, pp. 824-833, 2007.

[13] E. K. Dimitriadis, F. Horkay, J. Maresca, B. Kachar, and R. S. Chadwick, "Determination of elastic moduli of thin layers of soft material using the atomic force microscope," *Biophysical Journal,* vol. 82, pp. 2798-2810, May 2002.

[14] R. E. Mahaffy, S. Park, E. Gerde, J. Kas, and C. K. Shih, "Quantitative analysis of the viscoelastic properties of thin regions of fibroblasts using atomic force microscopy," *Biophysical Journal,* vol. 86, pp. 1777-1793, Mar 2004.

[15] A. Raman, S. Trigueros, A. Cartagena, A. P. Z. Stevenson, M. Susilo, E. Nauman, *et al.*, "Mapping nanomechanical properties of live cells using multi-harmonic atomic force microscopy," *Nature Nanotechnology,* vol. 6, pp. 809-814, Dec 2011.

[16] N. Gavara and R. S. Chadwick, "Determination of the elastic moduli of thin samples and adherent cells using conical atomic force microscope tips," *Nature Nanotechnology,* vol. 7, pp. 733-736, Nov 2012.

[17] M. J. Jaasma, W. M. Jackson, and T. M. Keaveny, "Measurement and characterization of whole-cell mechanical behavior," *Annals of Biomedical Engineering,* vol. 34, pp. 748-758, May 2006.

[18] K.L.Johnson, "Contact Mechnics," *Cambridge University Press*, 1985.

[19] F. Rico, P. Roca-Cusachs, N. Gavara, R. Farre, M. Rotger, and D. Navajas, "Probing mechanical properties of living cells by atomic force microscopy with blunted pyramidal cantilever tips," *Physical Review E,* vol. 72, Aug 2005.

[20] http://www.biology.arizona.edu/cell_bio/tutorials/cytoskeleton/page1.html

[21] A. J. Maniotis, C. S. Chen, and D. E. Ingber, "Demonstration of mechanical connections between integrins cytoskeletal filaments, and nucleoplasm that stabilize nuclear structure," *Proceedings of the National Academy of Sciences of the United States of America*, vol. 94, pp. 849-854, Feb 4 1997.

[22] F. M. Pavalko, N. X. Chen, C. H. Turner, D. B. Burr, S. Atkinson, Y. F. Hsieh, *et al.*, "Fluid shear-induced mechanical signaling in MC3T3-E1 osteoblasts requires cytoskeleton-integrin interactions," *American Journal of Physiology-Cell Physiology*, vol. 275, pp. C1591-C1601, Dec 1998.

[23] D. C. Lin, D. I. Shreiber, E. K. Dimitriadis, and F. Horkay, "Spherical indentation of soft matter beyond the Hertzian regime: numerical and experimental validation of hyperelastic models," *Biomechanics and Modeling in Mechanobiology*, vol. 8, pp. 345-358, Oct 2009.

[24] I. Kang, D. Panneerselvam, V. P. Panoskaltsis, S. J. Eppell, R. E. Marchant, and C. M. Doerschuk, "Changes in the hyperelastic properties of endothelial cells induced by tumor necrosis factor-alpha," *Biophysical Journal,* vol. 94, pp. 3273-3285, Apr 15 2008.

[25] M. Kauer, V. Vuskovic, J. Dual, G. Szekely, and M. Bajka, "Inverse finite element characterization of soft tissues," *Medical Image Analysis,* vol. 6, pp. 275-287, Sep 2002.

[26] E. Tonuk and M. B. Silver-Thorn, "Nonlinear elastic material property estimation of lower extremity residual limb tissues," *Ieee Transactions on Neural Systems and Rehabilitation Engineering,* vol. 11, pp. 43-53, Mar 2003.

[27] K. Miller and K. Chinzei, "Constitutive modelling of brain tissue: Experiment and theory," *Journal of Biomechanics,* vol. 30, pp. 1115-1121, Nov-Dec 1997.

[28] J. E. Miller-Young, N. A. Duncan, and G. Baroud, "Material properties of the human calcaneal fat pad in compression: experiment and theory," *Journal of Biomechanics,* vol. 35, pp. 1523-1531, Dec 2002.

[29] T. Hu and J. P. Desai, "Characterization of soft-tissue material properties: Large deformation analysis," *Medical Simulation, Proceedings,* vol. 3078, pp. 28-37, 2004.

[30] Y. Liu, A. E. Kerdok, and R. D. Howe, "A Nonlinear finite element model of soft tissue indentation," *Medical Simulation, Proceedings,* vol. 3078, pp. 67-76, 2004.

[31] S. Kasas, X. Wang, H. Hirling, R. Marsault, B. Huni, A. Yersin, *et al.*, "Superficial and deep changes of cellular mechanical properties following cytoskeleton disassembly," *Cell Motility and the Cytoskeleton,* vol. 62, pp. 124-132, Oct 2005.

[32] L. M. Zhao, D. Schaefer, H. X. Xu, S. J. Modi, W. R. LaCourse, and M. R. Marten, "Elastic properties of the cell wall of Aspergillus nidulans studied with atomic force microscopy," *Biotechnology Progress,* vol. 21, pp. 292-299, Jan-Feb 2005.

[33] Y. I. T.Ohashi, Y.Ishikawa, T.Matsumoto, and M.Sato, "Experimental and numerical analysis of local mechanical properties measured by atomic force microscopy for sheared endothelial cells," *Bio-Medical Materials and Engineering,* vol. 12, p. 9, 2002.